Two-dimensional semimetal states in transition metal trichlorides : a first-principles study

Two-dimensional semimetal states in transition metal trichlorides: A first-principles study

Yawei Yu,[1] Xiao Xie,[1] Xiaobiao Liu,[2] Jia Li,[1] François M. Peeters,[3,4] and Linyang Li[1,a)]

[1]*School of Science, Hebei University of Technology, Tianjin 300401, China*

[2]*School of Science, Henan Agricultural University, Zhengzhou 450002, China*

[3]*Departamento de Física, Universidade Federal do Ceará, Caixa Postal 6030, 60455-760 Fortaleza, Ceará, Brazil*

[4]*Department of Physics, University of Antwerp, Groenenborgerlaan 171, B-2020 Antwerp, Belgium*

[a)]Author to whom correspondence should be addressed: linyang.li@hebut.edu.cn

ABSTRACT

Two-dimensional (2D) transition metal trihalide (TMX_3, X = Cl, Br, I) family has attracted considerable attention in recent years due to the realizations of $CrCl_3$, $CrBr_3$, and CrI_3 monolayers. Up to now the main focus of the theoretically predicted TMX_3 monolayers has been on the Chern insulator states, which can realize the quantum anomalous Hall effect. Here, using first-principles calculations, we theoretically demonstrate that the stable $OsCl_3$ monolayer has a ferromagnetic ground state and a spin-polarized Dirac point without spin-orbit coupling (SOC), which disappears in the band structure of Janus $OsBr_{1.5}Cl_{1.5}$ monolayer. We find that $OsCl_3$ exhibits in-plane magnetization when SOC is included. By manipulating the magnetization direction along the C_2 symmetry axis of the $OsCl_3$ structure, a gapless half-Dirac semimetal state with SOC can be achieved, which is different from the gapped Chern insulator state. Both semimetal states of $OsCl_3$ monolayer without and with SOC exhibit a linear half-Dirac point (twofold degenerate) with high Fermi velocities. The achievement of the 2D semimetal state with SOC is expected to be found in other TMX_3 monolayers, and we confirm it in $TiCl_3$ monolayer. This provides a different perspective to study the band structure with SOC of the 2D TMX_3 family.

The story of two-dimensional (2D) intrinsic ferromagnetic (FM) material started with the realization of CrI_3 monolayer,[1] which provides an excellent platform for the investigation of quantum phenomena on magnetism. Similar to the definition of 2D transition metal dichalcogenide (TMD),[2] 2D transition metal trihalide (TMX_3, X = Cl, Br, and I) was proposed. From the theoretically calculated electronic band structures in the absence of spin-orbital coupling (SOC) effect, three FM types are interesting: (i) spin-polarized Dirac band structure around the Fermi level,[3-7] including $TiCl_3$,[8] VCl_3/VBr_3,[9-11] $FeCl_3$/$FeBr_3$/FeI_3,[12] $NiCl_3$,[13] RuI_3,[14] $PdCl_3$,[15] $OsCl_3$,[16] and $PtCl_3$;[17] (ii) semiconductors, including CrI_3[18] and MoI_3;[19] and (iii) half-metals, including OsI_3.[20] All three kinds of band structures play an important role in spintronic devices due to their intrinsic FM properties. Quantitatively, the spin-polarized Dirac band structure of the FM ground state has the advantage, which can be regarded as a half-Dirac semimetal state due to the twofold degenerate Dirac point.[21-23] These half-Dirac materials have received considerable attention lately due to their unique electronic properties. One of the important features is that the half-Dirac point resulting from two linear crossing bands can lead to a high Fermi velocity, which is promising for applications in high-speed electronic devices. In general, when SOC is taken into account, a nontrivial bandgap can be opened at the half-Dirac point, giving rise to a nontrivial Chern insulator state, and leading to the quantum anomalous Hall (QAH) effect.

Since only few experiments have been added to measure the QAH at ultra-low temperature,[24,25] the focus of most theoretical works on TMX_3 monolayers is to realize the opening of a bandgap at the spin-polarized Dirac (half-Dirac) point in order to achieve nontrivial Chern insulator states. However, besides the gapped band structure of Chern insulator states, the case of a gapless band structure in the presence of SOC should not be neglected,[17] corresponding to a semimetal state with SOC. The key to realize a gapless semimetal state is through the manipulation of the magnetization direction. For FM materials, the magnetization direction can modify the electronic band structure, which is a magneto band-structure

effect.[18] In theory, a direct-to-indirect bandgap transition and tunable topological states can be achieved in CrI_3 monolayer when in-plane magnetization is turned on.[18] In experiment, Bedoya-Pinto *et al.* constructed a nearly ideal system with in-plane magnetization, a $CrCl_3$ monolayer grown on graphene/6H-SiC (0001).[26] For the case of in-plane magnetization, each magnetization direction in the *xy* plane should be an easy magnetization direction, and its corresponding band structure should be studied.

The details of calculation method are given in Part I (supplementary material).[27-35] In this work, we firstly focus on a monolayer of transition metal trichloride, $OsCl_3$, which was originally proposed by Sheng *et al*.[16] The structure of monolayer $OsCl_3$ is illustrated in Fig. 1(a). It consists of an Os atomic layer sandwiched between two Cl atomic layers, where the Os atoms can form a honeycomb lattice. Based on this $OsCl_3$ structure, we further constructed a Janus structure by replacing the lower Cl atomic layer with a Br atomic layer. The Janus structure is also an important set of 2D materials,[36-40] which was first realized for MoSSe.[41-43] The structure of the Janus $OsBr_{1.5}Cl_{1.5}$ monolayer is shown in Fig. 1(b). The optimized lattice constant, Os-Cl bond length, and Cl-Cl distance along the vertical direction of the $OsCl_3$ monolayer are 6.05 Å, 2.38 Å, and 2.67 Å, respectively. As listed in Table 1, the Janus $OsBr_{1.5}Cl_{1.5}$ monolayer has a larger lattice constant (6.28 Å). The angle of Os-Cl-Os is 94.40° in the $OsCl_3$ monolayer, which is between the 92.49° of Os-Br-Os and the 98.64° of Os-Cl-Os in the Janus $OsBr_{1.5}Cl_{1.5}$ monolayer. These values of angle are close to the 95.5° of $CrCl_3$ monolayer.[44] The phonon spectra of the two monolayers were calculated, and all phonon frequencies were found to be real, implying their dynamical stability. For the energy stability of the two monolayers, their cohesive energies were calculated from the following formulae: $E_{coh}(OsCl_3) = (E_{Os2Cl6} - 2E_{Os} - 6E_{Cl})/8$ and $E_{coh}(OsBr_{1.5}Cl_{1.5}) = (E_{Os2Br3Cl3} - 2E_{Os} - 3E_{Br} - 3E_{Cl})/8$, where $E_{Os2Cl6}/E_{Os2Br3Cl3}$ is the total energy of the $OsCl_3/OsBr_{1.5}Cl_{1.5}$ monolayer (per unit cell) and $E_{Os}/E_{Cl}/E_{Br}$ is the total energy of a single Os/Cl/Br atom. The results of cohesive energy are shown in Table 1, and the negative values −3.59 eV/atom ($OsCl_3$) and −3.39 eV/atom (Janus $OsBr_{1.5}Cl_{1.5}$) indicate the energetic

stability of the systems.

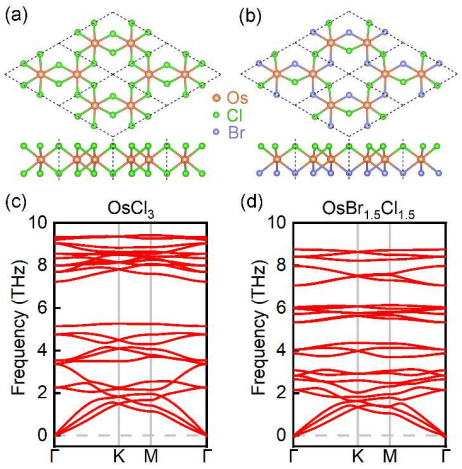

Fig. 1. Top and side views of (a) $OsCl_3$ monolayer and (b) Janus $OsBr_{1.5}Cl_{1.5}$ monolayer. The phonon spectra of (c) $OsCl_3$ monolayer and (d) Janus $OsBr_{1.5}Cl_{1.5}$ monolayer.

Table 1. The optimized lattice constant (a), Os-Cl/Os-Br bond length (l), thickness (h), and cohesive energy (E_{coh}, unit: eV/atom) for $OsCl_3$ and Janus $OsBr_{1.5}Cl_{1.5}$ monolayers. The total energy of the AFM-Z/AFM-S/AFM-N/NM phase relative to FM phase for $OsCl_3$ and Janus $OsBr_{1.5}Cl_{1.5}$ monolayers (unit: meV/Os).

Monolayer	a (Å)	l (Å)	h (Å)	E_{coh}	AFM-Z	AFM-S	AFM-N	NM
$OsCl_3$	6.05	2.38	2.67	−3.59	41.3	71.7	95.7	99.5
$OsBr_{1.5}Cl_{1.5}$	6.28	2.39 /2.51	2.73	−3.39	57.4	64.5	100.6	106.5

The two monolayers exhibit a FM ground state, and the calculation details are given in Part II (supplementary material).[16] Based on their FM ground state, we calculated the electronic band structures without SOC for the two monolayers in Fig. 2, where the blue/red curves correspond to the spin-up/spin-

down channel and a spin-splitting occurs between the two spin channels. For the $OsCl_3$ monolayer [Fig. 2(a)], there is a half-Dirac point at the Fermi level in the spin-down channel, which is located at the high-symmetry path M-Γ of the first Brillouin zone (BZ). The two bands forming the half-Dirac point are linear with the Fermi velocity of $0.54/1.41\times10^5$ m/s. We found that the five *d* atomic orbitals (d_{xy}, d_{yz}, d_{xz}, $d_{x^2-y^2}$, and d_{z^2}) of Os atoms are mostly responsible for the bands around the Fermi level, as shown in Part III (supplementary material). Thus, the $OsCl_3$ monolayer is a half-Dirac semimetal of *d*-state without SOC,[23] and is essentially different from the half-Dirac semimetal of *p*-state, such as Cd_2N_3/1T-YN_2/1T-LaN_2/1T-LuN_2.[23,45-48] For the band structure without SOC of the Janus $OsBr_{1.5}Cl_{1.5}$ monolayer [Fig. 2(b)], two bands in the spin-down channel are above the Fermi level, and the half-Dirac point disappears with opening an indirect bandgap of 31.4 meV, making the Janus $OsBr_{1.5}Cl_{1.5}$ monolayer a FM semiconductor. The opening of the bandgap can be attributed to the broken structural symmetry. The space group of the $OsCl_3$ monolayer is *P*-31*m* (162) while the space group of the Janus $OsBr_{1.5}Cl_{1.5}$ monolayer is *P*31*m* (157). In view of their main symmetry, the $OsCl_3$ monolayer has C_2 symmetry and mirror symmetry while the Janus $OsBr_{1.5}Cl_{1.5}$ monolayer has mirror symmetry without C_2 symmetry, where the same vertical mirror plane can be found. Here, we can conclude that the half-Dirac point is preserved by the C_2 symmetry rather than the mirror symmetry, which we will further confirm by manipulating the magnetization direction with SOC for $OsCl_3$ monolayer. Hence, in the following discussions on SOC effect, we will only focus on the $OsCl_3$ monolayer.

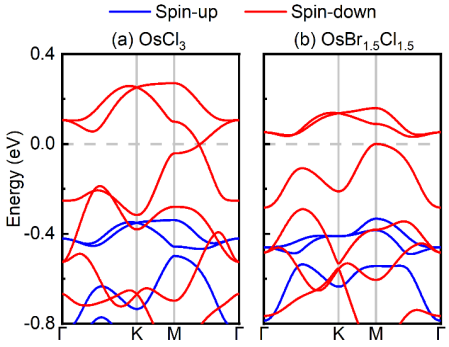

Fig. 2. Spin-polarized band structures of (a) $OsCl_3$ monolayer and (b) Janus $OsBr_{1.5}Cl_{1.5}$ monolayer. The blue (red) curves indicate the spin-up (spin-down) channel.

Magnetic anisotropy energy (MAE) mainly originates from the SOC effect, which can be evaluated from the total energy difference between the easy direction and the hard direction.[49] To evaluate the MAE of the $OsCl_3$ monolayer, we used two methods: relativistic self-consistent field (SCF) calculations with different orientations, and relativistic non-SCF calculations with different orientations.[50] Here, three magnetization directions are important, including 100, 010, and 001. By setting the MAE of 001 direction as a base (0), the MAE of the 100 direction was calculated by MAE (100) = E (100) – E (001) while the MAE of 010 direction was calculated by MAE (010) = E (010) – E (001). For the SCF method, the MAE of 100 (010) direction is −32.45 (−32.98) meV/Os. For the non-SCF method, the MAE of 100 (010) direction is −22.47 (−22.75) meV/Os. The two different methods show in-plane magnetization but there is a difference in the calculated values of MAE and magnetic moment. The non-SCF method cannot describe the change of magnetic moment due to the SOC effect, because it still gives 1 μ_B/Os in the 100/010/001 direction, which is the same value as without SOC. However, the magnetic moment becomes 0.7 μ_B/Os in the 100/010/001 direction when using the SCF method. Therefore, we believe that the results from SCF are more reasonable. Comparing the three values of MAE (100) = −32.45 meV/Os, MAE (010) = −32.98

meV/Os, and MAE (001) = 0, the magnetization along 001 direction is hard to achieve experimentally while the magnetization along 100/010 direction should be possible in experiment. The magnetization of 010 direction shows the lowest MAE (total energy), and its corresponding SOC band structure has been studied in detail in previous work.[16] Although the MAE (total energy) of 100 direction is 0.53 meV/Os higher than that of 010 direction, the magnetization of 100 direction can be tuned by using an external magnetic field, and therefore its corresponding band structure deserves to be studied.[51]

When the SOC effect is not included, there are six symmetrical half-Dirac points along the high-symmetry paths, M-M_3, M_1-M_4, and M_2-M_5, as shown in Part IV (supplementary material). At first, we used the magnetization direction $\hat{\boldsymbol{m}}$ along the 100 direction, corresponding to the angle $\varphi = 0°$ with respect to the positive direction of x axis [orange arrow in Fig. 3(a)]. The first BZ of the $OsCl_3$ monolayer is shown in Fig. 3(a), and the global band structure with SOC of the $OsCl_3$ monolayer for $\varphi = 0°$ is shown in Fig. 3(b). It is clear that there is a gapless point in the high-symmetry path M-Γ while another gapless point appears in the high-symmetry path Γ-M_3 [Fig. 3(c)], and the $\hat{\boldsymbol{m}}$ is parallel to MM_3. The gapless point formed by two linear bands is against SOC and twofold degenerate,[52,53] which can also be regarded as a half-Dirac point.[21,54] Its Fermi velocity is $0.48/1.13\times10^5$ m/s, almost equal to the value of $0.54/1.41\times10^5$ m/s without SOC. When the angle between $\hat{\boldsymbol{m}}$ and the positive direction of x axis is $\varphi = 180°$, the same band structure can be obtained as for the case of $\varphi = 0°$ [Figs. 3(b) and 3(c)]. The above two magnetization directions of $\hat{\boldsymbol{m}}$ ($\varphi = 0°$ and $\varphi = 180°$) correspond to the C_{2x} symmetry axis of the $OsCl_3$ structure. When the magnetization direction $\hat{\boldsymbol{m}}$ is parallel to the C_{2x} symmetry axis, the C_2 symmetry can be preserved and two half-Dirac points can be found in the corresponding parallel high-symmetry path M-M_3. According to the C_{3z} symmetry of the $OsCl_3$ monolayer, there are another two C_2 symmetry axes, C_{2+} and C_{2-} [Fig. 3 (a)]. For the case of $\varphi = 0°$ (180°), the C_2 symmetry is broken in the other two directions of the C_2 symmetry axis (C_{2+} and C_{2-}), leading to the absence of half-Dirac points in the corresponding parallel high-symmetry

paths M_1-M_4 and M_2-M_5 ($M_1M_4 \| C_{2+}$ and $M_2M_5 \| C_{2-}$) [Figs. 3(a) and 3(c)]. Considering the Hubbard U correction for the electronic correlation of d electrons, the two half-Dirac points can be preserved when the value of U is less than 0.2261 eV, as shown in Part V (supplementary material). Similarly, when the magnetization direction $\hat{\boldsymbol{m}}$ is parallel to the C_{2+}/C_{2-} symmetry axis of the $OsCl_3$ structure, corresponding to $\varphi = 60°$ (240°)/$\varphi = 120°$ (300°), the gapless half-Dirac points should appear again. For the case of $\varphi =$ 60° (240°) [Fig. 3(d)], when the magnetization directions $\hat{\boldsymbol{m}}$ is parallel to the C_{2+} symmetry axis, the C_2 symmetry along the direction of C_{2+} is preserved and two half-Dirac points can be found in the corresponding parallel high-symmetry path M_1-M_4, as shown in Figs. 3(e) and 3(f). For the case of $\varphi = 120°$ (300°) [Fig. 3(g)], when the magnetization directions $\hat{\boldsymbol{m}}$ is parallel to the C_{2-} symmetry axis, the C_2 symmetry is preserved along the direction of C_{2-} and two half-Dirac points can be found in the corresponding parallel high-symmetry path M_2-M_5, as shown in Figs. 3(h) and 3(i). Therefore, by forcing the magnetization direction along the C_2 symmetry axes of the $OsCl_3$ structure, including $\varphi = 0°$, 60°, 120°, 180°, 240°, and 300°, we are able to realize 2D gapless half-Dirac semimetal states with SOC.

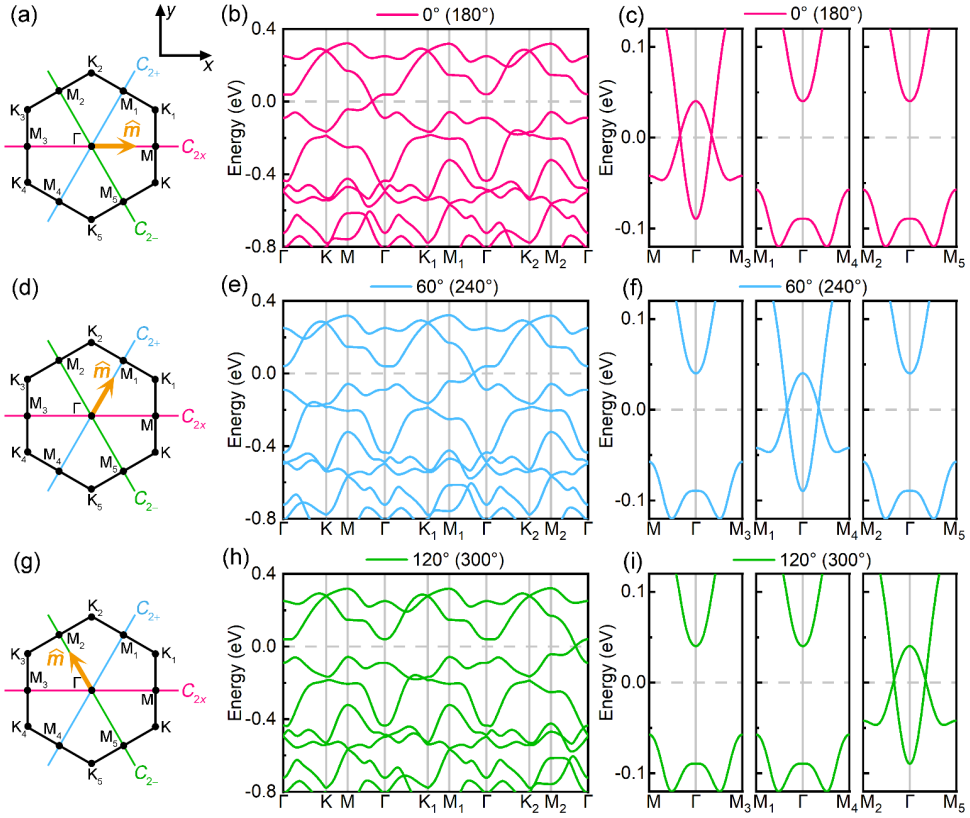

Fig. 3. Orange arrow indicates the magnetization directions of (a) $\varphi = 0°$, (d) $\varphi = 60°$, and (g) $\varphi = 120°$, where the pink, light blue, and green lines represent the C_{2x}, C_{2+}, and C_{2-} symmetry axis, respectively. Global band structures with SOC of the $OsCl_3$ monolayer for (b) $\varphi = 0°$ (180°), (e) $\varphi = 60°$ (240°), and (h) $\varphi = 120°$ (300°). Band structures with SOC along the high-symmetry path M-M_3/M_1-M_4/M_2-M_5 of the $OsCl_3$ monolayer for (c) $\varphi = 0°$ (180°), (f) $\varphi = 60°$ (240°), and (i) $\varphi = 120°$ (300°).

The 2D half-Dirac semimetal states with SOC are different from the Chern insulator states where the $\hat{\boldsymbol{m}}$ is along the magnetization direction that is not parallel to the C_2 symmetry axis of $OsCl_3$ structure. For the case of $\varphi = 90°$, we calculated the band structures with SOC, as shown in Part VI (supplementary

material). The gapless points disappear in all the three high-symmetry paths M-M_3, M_1-M_4, and M_2-M_5, and a global bandgap of 55.6 meV can be found, where the valence band maximum and conduction band minimum are marked with black dots. At each of the six half-Dirac points without SOC (Part IV, supplementary material), a bandgap is opened due to SOC with breaking the C_2 symmetry. This global bandgap is nontrivial, which can be further confirmed by the one edge state connecting the valence band area and conduction band area, corresponding to Chern number $|C|=1$ according to the bulk-edge correspondence. However, comparing the edge states for the six angles, φ = 0°, 60°, 120°, 180°, 240°, and 300°, we indeed observe a clear "Fermi arc" connecting the pair of gapless points, as shown in Figs. 4(a)-4(f), which is the main feature of semimetal states. In this $OsCl_3$ monolayer with SOC, the gapless half-Dirac semimetal states are due to the preservation of C_2 symmetry, which is similar in the case of LuN_2/YN_2/CrO_2/Na_2C monolayer with a 1T structure.[48,51,55,56] Besides the C_2 symmetry, the mirror symmetry can also realize the semimetal states with SOC. Since magnetization direction $\hat{\boldsymbol{m}}$ is an axial vector, it requires that $\hat{\boldsymbol{m}}$ is perpendicular to this mirror plane in order to preserve the mirror symmetry in the semimetal states with SOC, which have been realized in some theoretical monolayers, such as $PtCl_3$,[17] CsS,[57] and LaCl.[58] It should be noticed that this semimetal state is indeed against SOC effect, which is different from that under the premise of negligible SOC due to the light elements, such as in a phthalocyanine-based covalent organic framework.[59]

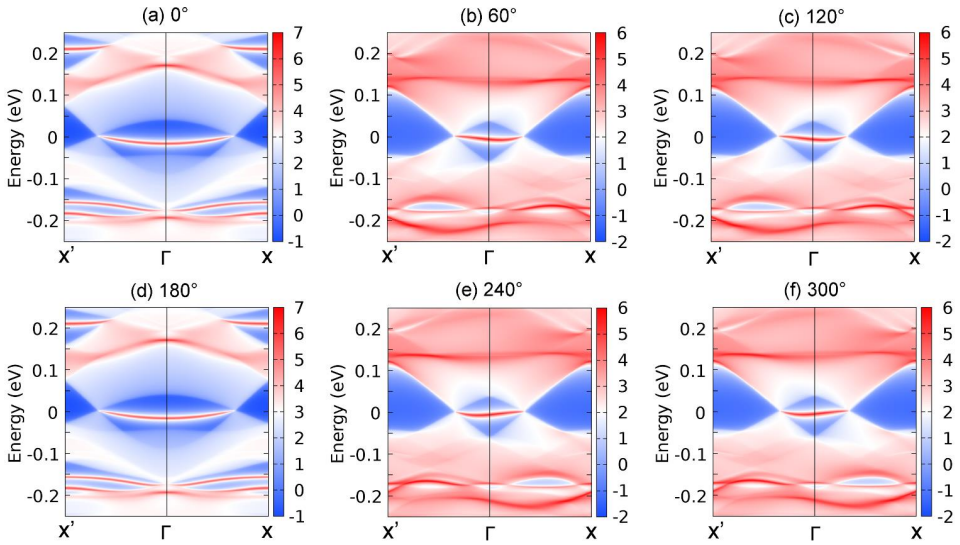

Fig. 4. Edge states of the $OsCl_3$ monolayer for (a) $\varphi = 0°$, (b) $\varphi = 60°$, (c) $\varphi = 120°$, (d) $\varphi = 180°$, (e) $\varphi = 240°$, and (f) $\varphi = 300°$.

So far, we have confirmed the 2D gapless semimetal states without and with SOC in the $OsCl_3$ monolayer. In the 2D TMX_3 family, there are many monolayers exhibiting a half-Dirac band structure without SOC. A natural question arises: Can we find the semimetal states with SOC in other 2D TMX_3 monolayers? Based on previous works on TMX_3 monolayers, the $TiCl_3$ monolayer also shows a half-Dirac point along the high-symmetry path M-Γ in the band structure without SOC,[8] exhibiting a half-Dirac semimetal state, and this result has been repeated in our calculations. Considering the SOC effect, the MAE of 100 direction can be calculated by MAE (100) = E (100) – E (001) while the MAE of 010 direction can be calculated by MAE (010) = E (010) – E (001). The MAE (100)/MAE (010) is −0.156/−0.156 meV/Ti, indicating in-plane magnetization. Then we calculated the band structures for the two magnetization directions (100 and 010). For the 100 direction [$\varphi = 0°$, Figs. 5(a) and 5(b)], the pair of two gapless half-Dirac points can be found in the high-symmetry path M-M_3 with preserving the same C_2 symmetry as in

the $OsCl_3$ monolayer, showing a 2D half-Dirac semimetal state with SOC [Fig. 5(c)]. A bandgap of 17.9 meV is opened at each half-Dirac point along the high symmetry path M_1-M_4/M_2-M_5 with breaking the C_2 symmetry. For the 010 direction [$\varphi = 90°$, Figs. 5(d) and 5(e)], a bandgap of 20.7/10.4/10.4 meV is opened at the half-Dirac point along the high symmetry path M-M_3/M_1-M_4/M_2-M_5, and each C_2 symmetry is broken, giving rise to a Chern insulator state with Chern number $|C| = 1$ according to the bulk-edge correspondence [Fig. 5(f)]. The above results ($\varphi = 0°$ and $\varphi = 90°$) of the $TiCl_3$ monolayer are similar to those of the $OsCl_3$ monolayer. Hence, we have proven that the 2D half-Dirac semimetal states in two monolayers of transition metal trichloride, $OsCl_3$ and $TiCl_3$, which originate from the preservation of C_2 symmetry. Further verification by performing experiments or employing more accurate calculations, such as based on DFT+DMFT (dynamical mean-field theory),[60] is necessary and left for future studies.

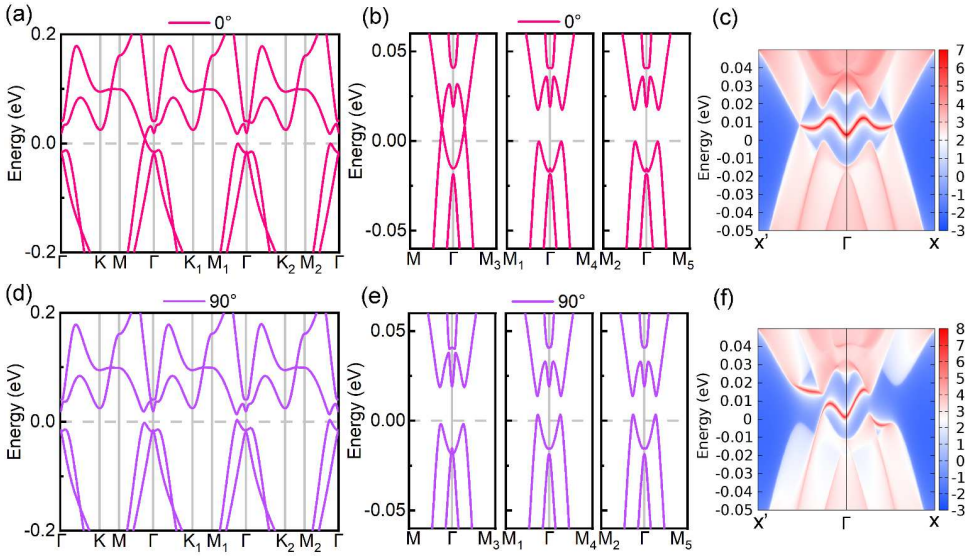

Fig. 5. Global band structures with SOC of the $TiCl_3$ monolayer for (a) $\varphi = 0°$ and (d) $\varphi = 90°$. Band structures with SOC along the high-symmetry path M-M_3/M_1-M_4/M_2-M_5 of the $TiCl_3$ monolayer for (b) $\varphi = 0°$ and (e) $\varphi = 90°$. Edge states of the $TiCl_3$ monolayer for (c) $\varphi = 0°$ and (f) $\varphi = 90°$.

In conclusion, the 2D half-Dirac semimetal states with SOC in the two monolayers of transition metal trichloride, $OsCl_3$ and $TiCl_3$, are shown by first-principles calculations. In the absence of SOC, the $OsCl_3$ monolayer is a FM half-Dirac semimetal and the Janus $OsBr_{1.5}Cl_{1.5}$ monolayer is a FM semiconductor, where the absence of the half-Dirac point should be attributed to the different structural symmetries between the two monolayers. We further confirmed it in $OsCl_3$ monolayer by considering the SOC effect. The gapless half-Dirac semimetal states can also be achieved in the $OsCl_3$ monolayer by manipulating the magnetization direction along the C_2 symmetry axis. Importantly, this type of 2D semimetal state with SOC can be further found in another monolayer of transition metal trichloride ($TiCl_3$). We establish a general rule to search for these 2D semimetal states with SOC, and introduce a different perspective to study the band structure with SOC of the 2D TMX_3 family.

See the supplementary material for calculation method (part I), magnetic property (part II), projected band structure of $OsCl_3$ (part III), band structure of $OsCl_3$ without SOC (part IV), band structure of $OsCl_3$ with U correction (part V), and Chern insulator state of $OsCl_3$ (part VI).

This work is supported by the National Natural Science Foundation of China (Grant No. 12004097), the Natural Science Foundation of Hebei Province (Grant No. A2020202031), and the Foundation for the Introduced Overseas Scholars of Hebei Province (Grant No. C20200313). X.L. acknowledges financial support from the National Natural Science Foundation of China (Grant No. 22005087). The computational resources utilized in this research were provided by Shanghai Supercomputer Center.

AUTHOR DECLARATIONS

Conflict of Interest

The authors have no conflicts to disclose.

DATA AVAILABILITY

The data that support the findings of this study are available from the corresponding author upon reasonable request.

REFERENCES

[1]B. Huang, G. Clark, E. Navarro-Moratalla, D. R. Klein, R. Cheng, K. L. Seyler, D. Zhong, E. Schmidgall, M. A. McGuire, D. H. Cobden *et al*., "Layer-dependent ferromagnetism in a van der Waals crystal down to the monolayer limit," Nature **546**, 270 (2017).

[2]M. Chhowalla, Z. Liu, and H. Zhang, "Two-dimensional transition metal dichalcogenide (TMD) nanosheets," Chem. Soc. Rev. **44**, 2584 (2015).

[3]X. L. Wang, "Proposal for a New Class of Materials: Spin Gapless Semiconductors," Phys. Rev. Lett. **100**, 156404 (2008).

[4]X.-L. Wang, "Dirac spin-gapless semiconductors: promising platforms for massless and dissipationless spintronics and new (quantum) anomalous spin Hall effects," Natl. Sci. Rev. **4**, 252 (2017).

[5]X. Wang, T. Li, Z. Cheng, X.-L. Wang, and H. Chen, "Recent advances in Dirac spin-gapless semiconductors," Appl. Phys. Rev. **5**, 041103 (2018).

[6]Z. Yue, Z. Li, L. Sang, and X. Wang, "Spin-Gapless Semiconductors," Small **16**, 1905155 (2020).

[7]X. Wang, Z. Cheng, G. Zhang, H. Yuan, H. Chen, and X.-L. Wang, "Spin-gapless semiconductors for future spintronics and electronics," Phys. Rep. **888**, 1 (2020).

[8]Z. Liu, G. Yang, X. Mao, L. Li, and J. Li, "Quantum anomalous Hall effect of Dirac half-metal monolayer

$TiCl_3$ with high Chern number," EPL **136**, 27004 (2021).

[9]J. Sun, X. Zhong, W. Cui, J. Shi, J. Hao, M. Xu, and Y. Li, "The intrinsic magnetism, quantum anomalous Hall effect and Curie temperature in 2D transition metal trihalides," Phys. Chem. Chem. Phys. **22**, 2429 (2020).

[10]J. He, S. Ma, P. Lyu, and P. Nachtigall, "Unusual Dirac half-metallicity with intrinsic ferromagnetism in vanadium trihalide monolayers," J. Mater. Chem. C **4**, 2518 (2016).

[11]Y. Li, Y. Liu, C. Wang, J. Wang, Y. Xu, and W. Duan, "Electrically tunable valleytronics in quantum anomalous Hall insulating transition metal trihalides," Phys. Rev. B **98**, 201407(R) (2018).

[12]P. Li, "Prediction of intrinsic two dimensional ferromagnetism realize quantum anomalous Hall effect," Phys. Chem. Chem. Phys. **21**, 6712 (2019).

[13]J. He, X. Li, P. Lyu, and P. Nachtigall, "Near-room-temperature Chern insulator and Dirac spin-gapless semiconductor: nickel chloride monolayer," Nanoscale **9**, 2246 (2017).

[14]C. Huang, J. Zhou, H. Wu, K. Deng, P. Jena, and E. Kan, "Quantum anomalous Hall effect in ferromagnetic transition metal halides," Phys. Rev. B **95**, 045113 (2017).

[15]Y.-p. Wang, S.-s. Li, C.-w. Zhang, S.-f. Zhang, W.-x. Ji, P. Li, and P.-j. Wang, "High-temperature Dirac half-metal $PdCl_3$: a promising candidate for realizing quantum anomalous Hall effect," J. Mater. Chem. C **6**, 10284 (2018).

[16]X.-L. Sheng and B. K. Nikolić, "Monolayer of the 5*d* transition metal trichloride $OsCl_3$: A playground for two-dimensional magnetism, room-temperature quantum anomalous Hall effect, and topological phase transitions," Phys. Rev. B **95**, 201402(R) (2017).

[17]J.-Y. You, C. Chen, Z. Zhang, X.-L. Sheng, S. A. Yang, and G. Su, "Two-dimensional Weyl half-semimetal and tunable quantum anomalous Hall effect," Phys. Rev. B **100**, 064408 (2019).

[18]P. Jiang, L. Li, Z. Liao, Y. X. Zhao, and Z. Zhong, "Spin Direction-Controlled Electronic Band Structure

in Two-Dimensional Ferromagnetic CrI_3," Nano Lett. **18**, 3844 (2018).

[19]J. Zhang, B. Zhao, C. Ma, and Z. Yang, "Bipolar ferromagnetic semiconductors and doping-tuned room-temperature half-metallicity in monolayer MoX_3 (X = Cl, Br, I): An HSE06 study," Phys. Rev. B **103**, 075433 (2021).

[20]B. G. Li, Y. F. Zheng, H. Cui, P. Wang, T. W. Zhou, D. D. Wang, H. Chen, and H. K. Yuan, "First-principles investigation of a new 2D magnetic crystal: Ferromagnetic ordering and intrinsic half-metallicity," J. Chem. Phys. **152**, 244704 (2020).

[21]M. Wu, Z. Wang, J. Liu, W. Li, H. Fu, L. Sun, X. Liu, M. Pan, H. Weng, M. Dincă *et al*., "Conetronics in 2D metal-organic frameworks: double/half Dirac cones and quantum anomalous Hall effect," 2D Mater. **4**, 015015 (2017).

[22]Y. Li, J. Li, Y. Li, M. Ye, F. Zheng, Z. Zhang, J. Fu, W. Duan, and Y. Xu, "High-Temperature Quantum Anomalous Hall Insulators in Lithium-Decorated Iron-Based Superconductor Materials," Phys. Rev. Lett. **125**, 086401 (2020).

[23]X.-Y. Li, W.-X. Ji, P.-J. Wang, and C.-W. Zhang, "Half-Dirac semimetals and the quantum anomalous Hall effect in Kagome Cd_2N_3 lattices," Nanoscale Adv. **3**, 847 (2021).

[24]C.-Z. Chang, J. Zhang, X. Feng, J. Shen, Z. Zhang, M. Guo, K. Li, Y. Ou, P. Wei, L.-L. Wang *et al*., "Experimental Observation of the Quantum Anomalous Hall Effect in a Magnetic Topological Insulator," Science **340**, 167 (2013).

[25]Y. Deng, Y. Yu, M. Z. Shi, Z. Guo, Z. Xu, J. Wang, X. H. Chen, and Y. Zhang, "Quantum anomalous Hall effect in intrinsic magnetic topological insulator $MnBi_2Te_4$," Science **367**, 895 (2020).

[26]A. Bedoya-Pinto, J.-R. Ji, A. K. Pandeya, P. Gargiani, M. Valvidares, P. Sessi, J. M. Taylor, F. Radu, K. Chang, and S. S. P. Parkin, "Intrinsic 2D-XY ferromagnetism in a van der Waals monolayer," Science **374**, 616 (2021).

[27]G. Kresse and J. Hafner, "*Ab initio* molecular dynamics for open-shell transition metals," Phys. Rev. B **48**, 13115 (1993).

[28]G. Kresse and J. Furthmüller, "Efficient iterative schemes for *ab initio* total-energy calculations using a plane-wave basis set," Phys. Rev. B **54**, 11169 (1996).

[29]G. Kresse and D. Joubert, "From ultrasoft pseudopotentials to the projector augmented-wave method," Phys. Rev. B **59**, 1758 (1999).

[30]J. P. Perdew, K. Burke, and M. Ernzerhof, "Generalized Gradient Approximation Made Simple," Phys. Rev. Lett. **77**, 3865 (1996).

[31]A. Togo and I. Tanaka, "First principles phonon calculations in materials science," Scr. Mater. **108**, 1 (2015).

[32]M. P. López Sancho, J. M. López Sancho, and J. Rubio, "Highly convergent schemes for the calculation of bulk and surface Green functions," J. Phys. F: Met. Phys. **15**, 851 (1985).

[33]A. A. Mostofi, J. R. Yates, Y.-S. Lee, I. Souza, D. Vanderbilt, and N. Marzari, "wannier90: A tool for obtaining maximally-localised Wannier functions," Comput. Phys. Commun. **178**, 685 (2008).

[34]A. A. Mostofi, J. R. Yates, G. Pizzi, Y.-S. Lee, I. Souza, D. Vanderbilt, and N. Marzari, "An updated version of wannier90: A tool for obtaining maximally-localised Wannier functions," Comput. Phys. Commun. **185**, 2309 (2014).

[35]Q. S. Wu, S. N. Zhang, H.-F. Song, M. Troyer, and A. A. Soluyanov, "WannierTools: An open-source software package for novel topological materials," Comput. Phys. Commun. **224**, 405 (2018).

[36]M. Yagmurcukardes, Y. Qin, S. Ozen, M. Sayyad, F. M. Peeters, S. Tongay, and H. Sahin, "Quantum properties and applications of 2D Janus crystals and their superlattices," Appl. Phys. Rev. **7**, 011311 (2020).

[37]H. Sun, S.-S. Li, W.-x. Ji, and C.-W. Zhang, "Valley-dependent topological phase transition and quantum

anomalous valley Hall effect in single-layer RuClBr," Phys. Rev. B **105**, 195112 (2022).

[38]R. Li, J. Jiang, X. Shi, W. Mi, and H. Bai, "Two-Dimensional Janus FeXY (X, Y = Cl, Br, and I, X ≠ Y) Monolayers: Half-Metallic Ferromagnets with Tunable Magnetic Properties under Strain," ACS Appl. Mater. Interfaces **13**, 38897 (2021).

[39]S. Qi, J. Jiang, X. Wang, and W. Mi, "Valley polarization, magnetic anisotropy and Dzyaloshinskii-Moriya interaction of two-dimensional graphene/Janus 2H-VSe*X* (*X* = S, Te) heterostructures," Carbon **174**, 540 (2021).

[40]R. Li, J. Jiang, W. Mi, and H. Bai, "Room temperature spontaneous valley polarization in two-dimensional FeClBr monolayer," Nanoscale **13**, 14807 (2021).

[41]X. Tang and L. Kou, "2D Janus Transition Metal Dichalcogenides: Properties and Applications," Phys. Status Solidi B **259**, 2100562 (2022).

[42]A.-Y. Lu, H. Zhu, J. Xiao, C.-P. Chuu, Y. Han, M.-H. Chiu, C.-C. Cheng, C.-W. Yang, K.-H. Wei, Y. Yang *et al*., "Janus monolayers of transition metal dichalcogenides," Nat. Nanotech. **12**, 744 (2017).

[43]J. Zhang, S. Jia, I. Kholmanov, L. Dong, D. Er, W. Chen, H. Guo, Z. Jin, V. B. Shenoy, L. Shi *et al*., "Janus Monolayer Transition-Metal Dichalcogenides," ACS Nano **11**, 8192 (2017).

[44]F. Xue, Y. Hou, Z. Wang, and R. Wu, "Two-dimensional ferromagnetic van der Waals $CrCl_3$ monolayer with enhanced anisotropy and Curie temperature," Phys. Rev. B **100**, 224429 (2019).

[45]Z. Liu, J. Liu, and J. Zhao, "YN_2 monolayer: Novel p-state Dirac half metal for high-speed spintronics," Nano Res. **10**, 1972 (2017).

[46]X. Kong, L. Li, O. Leenaerts, W. Wang, X.-J. Liu, and F. M. Peeters, "Quantum anomalous Hall effect in a stable 1T-YN_2 monolayer with a large nontrivial bandgap and a high Chern number," Nanoscale **10**, 8153 (2018).

[47]L. Li, X. Kong, X. Chen, J. Li, B. Sanyal, and F. M. Peeters, "Monolayer 1T-LaN_2: Dirac spin-gapless

semiconductor of *p*-state and Chern insulator with a high Chern number," Appl. Phys. Lett. **117**, 143101 (2020).

[48]Y. Yu, X. Chen, X. Liu, J. Li, B. Sanyal, X. Kong, F. M. Peeters, and L. Li, "Ferromagnetism with in-plane magnetization, Dirac spin-gapless semiconducting properties, and tunable topological states in two-dimensional rare-earth metal dinitrides," Phys. Rev. B **105**, 024407 (2022).

[49]X.-Y. Li, M.-H. Zhang, M.-J. Ren, and C.-W. Zhang, "Emergence of 2D high-temperature nodal-line half-metal in monolayer AgN," Phys. Chem. Chem. Phys. **22**, 27024 (2020).

[50]X. Chen, Y. Liu, and B. Sanyal, "Manipulation of Electronic and Magnetic Properties of 3d Transition Metal (Cr, Mn, Fe) Hexamers on Graphene with Vacancy Defects: Insights from First-Principles Theory," J. Phys. Chem. C **124**, 4270 (2020).

[51]L. Jin, L. Wang, X. Zhang, Y. Liu, X. Dai, H. Gao, and G. Liu, "Fully spin-polarized Weyl fermions and in/out-of-plane quantum anomalous Hall effects in a two-dimensional d^0 ferromagnet," Nanoscale **13**, 5901 (2021).

[52]Z. Liu, W. Feng, H. Xin, Y. Gao, P. Liu, Y. Yao, H. Weng, and J. Zhao, "Two-dimensional spin-valley-coupled Dirac semimetals in functionalized SbAs monolayers," Mater. Horiz. **6**, 781 (2019).

[53]Z. Liu, L. Li, L. Cui, Y. Shi, T. Song, J. Cai, X. Cui, X. Jiang, and J. Zhao, "Intrinsic spin-valley-coupled Dirac state in Janus functionalized β-BiAs monolayer," Nanoscale Horiz. **6**, 283 (2021).

[54]X. Ma, L. Sun, J. Liu, and M. Zhao, "Floquet-engineered half-valley-metal state in two-dimensional gapped Dirac materials," Phys. Rev. B **104**, 155439 (2021).

[55]S. He, P. Zhou, Y. Yang, W. Wang, and L. Z. Sun, "1T-CrO_2 monolayer: a high-temperature Dirac half-metal for high-speed spintronics," Nanoscale Adv. **3**, 3093 (2021).

[56]W.-X. Ji, B.-M. Zhang, S.-F. Zhang, C.-W. Zhang, M. Ding, P.-J. Wang, and R. Zhang, "Na_2C monolayer: a novel 2p Dirac half-metal with multiple symmetry-protected Dirac cones," Nanoscale **10**, 13645 (2018).

[57]X. Zhou, R.-W. Zhang, Z. Zhang, D.-S. Ma, W. Feng, Y. Mokrousov, and Y. Yao, "Fully Spin-Polarized Nodal Loop Semimetals in Alkaline Metal Monochalcogenide Monolayers," J. Phys. Chem. Lett. **10**, 3101 (2019).

[58]Z. Liu, G. Zhao, B. Liu, Z. F. Wang, J. Yang, and F. Liu, "Intrinsic Quantum Anomalous Hall Effect with In-Plane Magnetization: Searching Rule and Material Prediction," Phys. Rev. Lett. **121**, 246401 (2018).

[59]X. Ni, H. Huang, and J.-L. Brédas, "Emergence of a Two-Dimensional Topological Dirac Semimetal Phase in a Phthalocyanine-Based Covalent Organic Framework," Chem. Mater. **34**, 3178 (2022).

[60]H. Zhang, K. Haule, and D. Vanderbilt, "Metal-Insulator Transition and Topological Properties of Pyrochlore Iridates," Phys. Rev. Lett. **118**, 026404 (2017).

PLEASE CITE THIS ARTICLE AS DOI: 10.1063/5.0105605

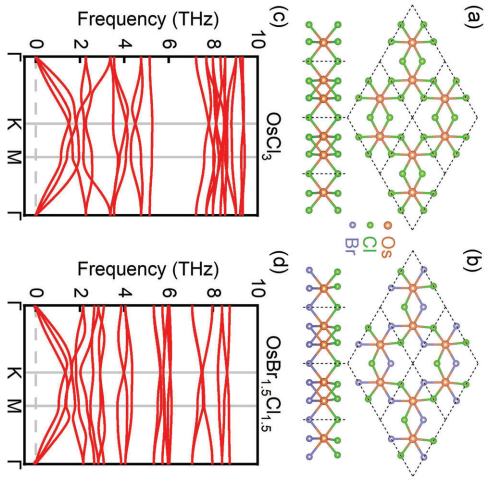

PLEASE CITE THIS ARTICLE AS DOI: 10.1063/5.0105605